EXPERIMENTAL AND NUMERICAL ANALYSIS OF MODE I INTERLAMINAR DELAMINATION OF A STITCHED LAMINATED COMPOSITE

Lotfi Hamitouche*, Mostapha Tarfaoui*, Alain Vautrin**
***MSN, ENSIETA, Brest– France, **Ecole des Mines de Saint-Etienne- France**

Keywords: *Delamination, Mode I, Stitching, Cohesive model*

Abstract

In this paper, mode I interlaminar fracture in stitched reinforced composite laminates is modelled using a cohesive model. The test configuration used in this study is a stitched reinforced double cantilever beam specimen. A bilinear damage-rate-dependent cohesive traction–separation law is adopted to model the woven composite fracture and discrete nonlinear spring elements to represent the stitches effect. A novel macroscopic law adopted from a 1D micromechanical-stitching model, is developed to model the stitches effect along the interface. The numerical simulations of DCB test with the present model, shows a good agreement with the experimental results.

1 Introduction

Fibre-reinforced laminate have very high in-plane strength and stiffness, but they usually exhibit low interlaminar fracture toughness, which make them sensitive to delamination. A single or repeated application of impact load may result in considerable damage in the form of delamination. Various techniques have therefore been considered to enhance damage tolerance by increasing the resistance of delamination to growth. One of the most effective ways of increasing the interlaminar fracture toughness is through-the-thickness reinforcement. Three dimensional fabric structures formed by braiding, weaving or transverse stitching processes have shown an effective way to reduce delamination [1-4]. The production of 3-D composites by weaving or braiding requires some special techniques; which are expensive to be used on shipyards superstructures. However, the concept of through-thickness reinforcement by using stitching process is much easier to fabricate and seems promising.

The effect of stitching is most important on mode I fracture and the best way to obtain this fracture mode into quasi-static loading conditions is through the double-cantilever-beam (D.C.B) specimen geometry.

In this paper, we implement discrete and continuous cohesive element aimed at modelling the delamination response in stitches reinforced composite laminates. Special interfacial elements referred to as cohesive elements are used to model the spontaneous initiation and propagation of the delamination crack. A 1D micromechanical model is developed to define a stitches response. These obtained law is used to model individual stitches as discrete nonlinear springs.

This work is directed along two axes. On the one hand, a numerical work is undertaken for the modelling of initiation and propagation of delamination in stitched and unstitched laminated composite. A bilinear damage-dependent cohesive traction separation law with a viscous regularization [5] was adopted to model the fracture of the un-reinforced composite. Discrete nonlinear springs with micromechanical-based behaviour were developed to present the stitching effect.

In the other hand, an experimental work is undertaken on the quantification of the stitch contribution on the delamination strength. For that, DCB tests are realized on two types of samples: standards without stitch and others with lightly stitched reinforcements.

In the last part of this paper, we perform mode I simulation and the results are compared with experimental data where, the validity of the model is discussed for a few generalized cases.

2 Stitch model

A micromechanics-based model have been developed to predict the effect of stitching on mode I delamination toughness. In this model, one considers representative elementary volume (R.E.V) defined by: fibre crossing the thickness, surrounded by resin (matrix) and maintained on two levels, the nod and the change of direction of fibre, Fig. 1. The basic assumptions for the stitches in this model are briefly reviewed.

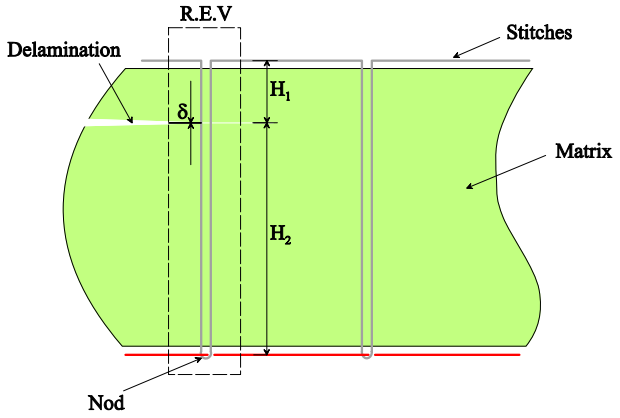

Fig. 1. Illustration of a stitch cross-section

2.1 Micromechanical assumptions

The stitch thread is assumed to be circular of cross-section. This simple model, considers the coupling between the slip interfacial fibre/matrix and the conditions of maintains fibre, Fig. 2.

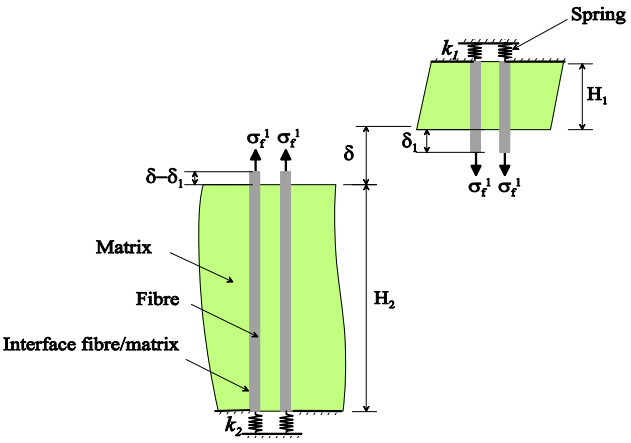

Fig. 2. Micromechanics of model

The physical parameters and the assumptions of the model are listed below:

- The fibre behaviour is assumed as elastic fragile, isotropic and a cylinder form (diameter d_f). With a Young modulus E_f and a null Poisson's ratio. During slipping stage, the abrasive effect of fibre is neglected.
- Elastic adhesion between fibre and matrix is neglected. At the time of slip, only the frictional shear stress τ at the matrix/thread interface is considered. The elastic bond strength is completely neglected. This assumption is the strongest of the model.
- The deformation in the matrix is also assumed to be negligible.
- The effect of the continuity and the change of direction of fibre drowned in the matrix of the composite is modelled by a linear spring with an elastic rigidity k_1. Thus, the effect of the node (loop) on fibre is represented by a spring with an elastic rigidity k_2.
- The tensile strength of stitching thread is assumed to be single, σ_{fu}.

From the assumptions enumerated above, one can determine the response of fibre subjected to an axial interface displacement δ.

2.2 Response of the stitch model

In order to simplify the mechanical problem presented on Fig. 2. one proposes to subdivide the stitch model in two parts *i* (i=1,2). The coupling between each part *i* is ensured by the equations of continuity of the stresses and displacements. One consider that the pull-out of a thread can be analyzed in tow parts : before slippage of embedded end or before spring activation and, after slippage of embedded end begins. The slippage distance of the fibre embedded end is denoted $S_i(0)$ (displacement of spring), the relative displacement between matrix and thread is δ_i and the axial fibre end stress is σ_{f1}. H_i is the embedded length of the thread in a matrix for each part i as shown in Fig. 2. The procedure of resolution of the mechanical problem shown in Fig. 2 is not developed in this paper, which will be the object of a future publication.

For our first example, we show the response of the model while varying the spring rigidity k_i of each part i, with $k_1 = k_2$. The physical characteristics of the stitch model are presented in table 1.

Table 1. Micromechanical properties of the stitch model

τ (MPa)	E_f (MPa)	d_f (mm)
10	125×10^3	0.3

It is supposed that the embedded length of the thread in two parts are equal, $H_1 = H_2 = 2$mm. Also, the failure criterion is activated and the ultimate tensile strength of the stitch is $\sigma_{fu} = 1.5$GPa. In Fig. 3 we show stitch bridge law (end-fibre stress, dimensionless displacement relationship) with the material properties and geometrical sizes given above.

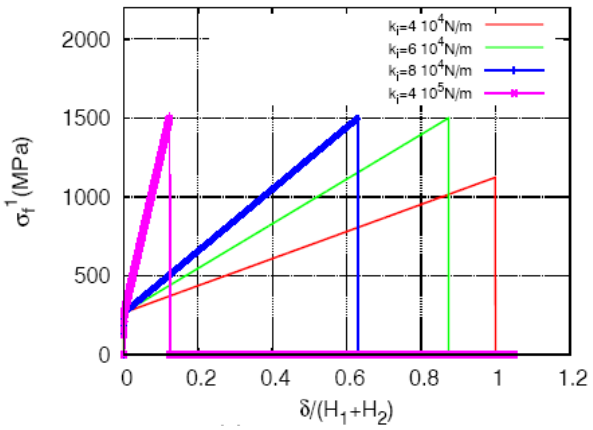

Fig. 3. Response of the micromechanical model

It can be seen that end-fibre stress keeps increases with an interface dimensionless displacement before the stitch breaks. The apparent rigidity of the model increases with the elastic rigidity of the springs. The stages of the model response are : before spring activation (fibre elasticity), the beginning of the slippage of embedded end and the break of a fibre.

2.4 Macro mechanical model

One interests in this part in a macroscopic behaviour law, which describe the micromechanical response of the stitch model, presented above. The stitch bridge law can be assimilated as elastic, plastic with no compression. Fig. 4. shows a macroscopic behaviour law used to model individual stitches. The elasto-plastic no compression law relies on two couples of parameters : yield coordinates (ε_y, σ_y) that correspond to the final elastic stage, and failure coordinates (ε_r, σ_r), characterizing the complete failure of the thread. Theses parameters can be estimated with a micromechanics tests and theses relations can not be defined explicitly.

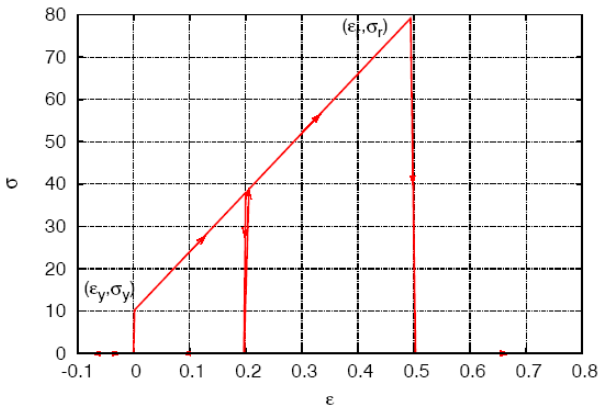

Fig. 4. elasto-plastic no compression law for a point decohesion element used to model individual stitches.

This behaviour law was implemented on implicit ABAQUS v6.5 [6] finite element code for a 1-D nonlinear spring elements.

3 cohesive model

A key component of the numerical model is the cohesive traction–separation relations used to model material failure in the unreinforced and reinforced regions. The cohesive failure model assumes the failure to occur over a strip-like cohesive zone immediately ahead of the crack tip. A bilinear rate and damage dependent traction–separation law for the cohesive zone is implemented to model the mid-surface delamination failure in the DCB specimens as shown in Fig. 5.

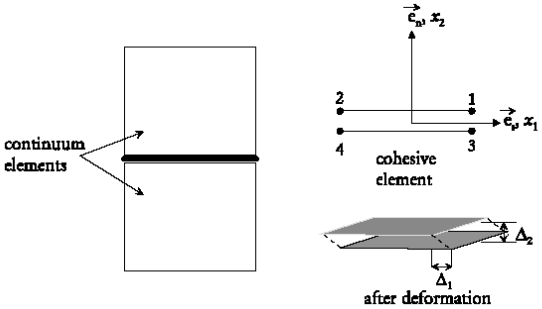

Fig. 5. Interfacial representation

The bilinear formulation presented in this section is based on the works of Geubelle and Baylor [7]. This particular model describes a bilinear relationship between the traction and the displacement jump, and is applied to the problem of delamination in composite laminates and in modelling glue joints. The continuous cohesive model is based on damage mechanics and on the linear mechanics of cracking failure.

The majority of cohesive zone laws have a coupling between normal and tangential directions. One can define the equivalent displacement jump. This parameter is the norm of the displacement jump vector, and it is used to compare different stages of the displacement jump state so that it is possible to define such concepts as 'loading', 'unloading' and 'reloading'. The equivalent displacement jump is a non-negative and continuous function, in Mazras [8] sens, defined as:

$$\delta = \sqrt{\alpha^2\left(\Delta_1^2 + \Delta_2^2\right) + \left\langle \Delta_3 \right\rangle_+^2} \quad ; \text{with } \alpha^2 = k_s / k_n \qquad (1)$$

Within the framework of Claussius-Duhem inequality, it is possible to impose restrictions on damage variable *d*. One can assume the irreversibility of damage process for any material point such as $\dot{d} \geq 0$, which avoids a physical phenomenon. The evolution of the damage is represented by an increasing scalar function defined by Turon et al. [9]:

$$d(\delta) = \begin{cases} 0 & si \quad \delta < \delta_0 \\ \dfrac{\delta_f(\delta - \delta_0)}{\delta(\delta_f - \delta_0)} & si \quad \delta_0 \leq \delta < \delta_f \\ 1 & si \quad \delta \geq \delta_f \end{cases} \qquad (2)$$

δ_0 is the onset displacement jump, it represents the value for which the damage starts. The initial damage threshold is obtained from the formulation of the initial damage surface or initial damage criterion. δ_f is the final displacement jump, it represents the value for which the material is completely damaged. It is obtained from the formulation of the propagation surface or propagation criterion.

3.1 Criterion of the onset of delamination

When the interface is subjected to pure I, or II loading Modes, the delamination occurs if the interlaminar associated stress reaches its maximum interfacial value. Obviously, under mixed-Mode loading, delamination onset may occur before those maximum values are obtained. The interaction between the stress components under mixed-Mode loading has to be taken into account by using a multi-axial stress criterion given as:

$$\left(\frac{t_1}{t_1^0}\right)^2 + \left(\frac{\langle t_2 \rangle_+}{t_2^0}\right)^2 = 1 \qquad (3)$$

where t_2^0 and t_1^0 are maximum interlaminar traction component associated with x_2 and x_1 directions. These parameters can be put linearly in equation with their respective displacement Δ_2^0 and Δ_1^0 ($\Delta_i^0 \geq 0; i = 1,2$).

3.2 Propagation criterion

Delamination propagates when the energy release rate equals its critical value under pure Mode I or Mode II fracture. Generally, delamination growth occurs under mixed-mode loading. In that case, the delamination process may take place before any of the energy release rate components attains its individual critical value. The most widely used criterion to predict propagation of delamination under mixed-Mode loading is the power law criterion based on the proposal of Reeder [10]:

$$\left(\frac{G_I}{G_{Ic}}\right)^n + \left(\frac{G_{II}}{G_{IIc}}\right)^n = 1 \qquad (4)$$

where *n* is an experimental parameter translating the existing coupling between the modes, G_{ic} is the critical energy release rate for mode *i* (*i* =I,II).

Quadratic solid plane element with four nodes and two Gaussian points have been selected for the numerical model. The implementation of the bilinear behaviour has been carried out as user element subroutine (UEL) in ABAQUS Standard v6.5 [6]. Using a various step size and Newton-Raphson algorithm has performed computations.

3.3 Localization problem

The instability due to the constitutive cohesive law $(t - \Delta)$ poses a real problem for the implicit finite elements code. Indeed, the use of Newton-Raphson methods of resolutions for problems presenting unstable branches of solutions can prove to be useless. This instability doesn't affect the uniqueness of FEM solution but induces a response discontinuity that we call "solution jump". To suppress this problem, the bilinear softening law can be affected by a viscous parameter. In the present model, the expression of the damage variable *d* is changed and it depends on the displacement jump rate [5]. The dependent rate cohesive model allows

us to overcome this difficulty and to obtain the convergence of the Newton-Raphson scheme.

4 Experimental study

DCB tests are usually performed to acquire information on the resistance to crack propagation in Mode I. This resistance is characterized by the critical energy release rate G_{Ic}. The tests are carried out on both unstitched and stitched laminate DCB specimens. Fig. 6. shows a schematic of the stitch reinforced DCB specimen. There is an unreinforced region of length L_d between the initial crack tip and the beginning of the reinforced region. Although in the reinforced region the density of stitches is different according to the thickness thus, one can see the effect of the stitching.

All specimens are glass taffetas fabric vinylester DION 9102 matrix reinforced laminated composites. They are 4 mm (10 plies) thick, 21.36mm wide and 176 mm long. A thin Teflon film is utilized to pre-crack the mid-plane of the laminate, the pre-crack initial length is a_0 (Fig. 6). A uniaxial testing system mounted on a LLYOD 1kN max. load testing machine is operated in displacement control mode, the crosshead speed is 1mm/min, and a computer-based data acquisition system is used. The crack tip progression is monitored by painting the side of the specimen with a white correction fluid and scored at 1mm intervals with a thin blade. During the test, the load-displacement curve is monitored and the crack lengths are continuously measured with a numerical camera (resolution 1280*x*960 pixels, frame rate 7.5 fps) equipped with a *x*8 zoom.

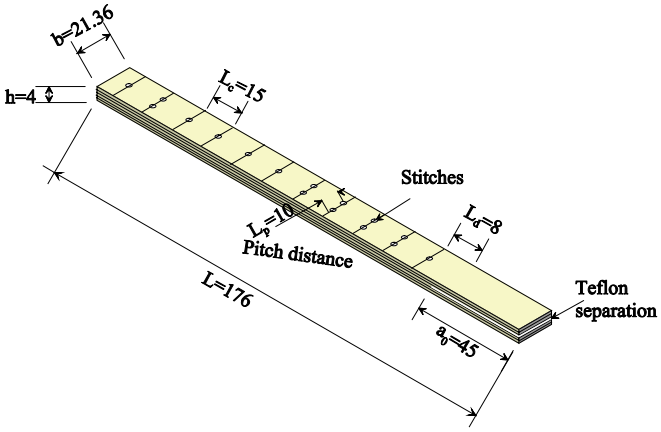

Fig. 6. Stitched DCB specimen geometry

4.1 Tests results

Three different methods can be utilized to calculate the Mode I fracture toughness according to ASTM standards [11]: the Compliance Calibration method (CC), the Modified Compliance Calibration method (MCC) and the Modified Beam Theory method (MBT) for both stitched and unstitched specimens. The initiation experimental values of fracture toughness G_{Ii} is depending on the specimens because it is strongly linked to the local crack tip conditions. The critical energy release rates are systematically estimated by those three previous methods. The G_{Ii} for crack initiation and G_{Ic} for critical crack propagation of the unreinfoced and reinforced through the thickness laminates are given in Figs. 7 and 8. It can be seen from these figures that the lightly stitched laminate has a higher G_{Ic} than the unstitched one ($G_{Ic}(stitched) = 1.5 \times G_{Ic}(unstitched)$) whereas, the values of G_{Ii} are approximately identical.

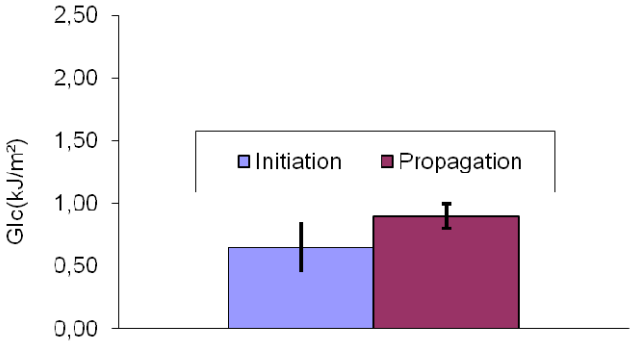

Fig. 7. Energy release rate for the unstitched DCB specimen

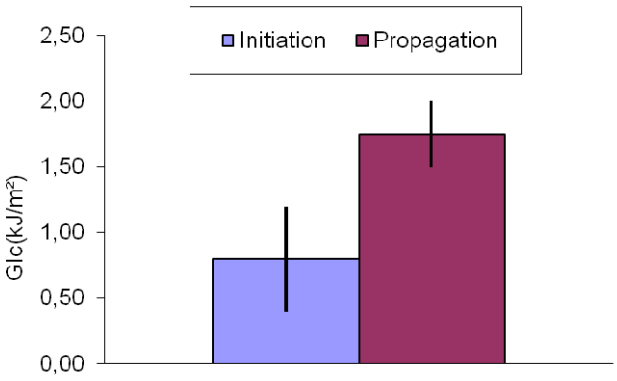

Fig. 8. Energy release rate for the stitched DCB specimen

5 FEA – experimental correlation

A 2D 4-node decohesion element is used to simulate mode I fracture toughness tests on the unstitched woven vinylester glass-fibre-reinforced

composite. For the stitched DCB specimen a cohesive zone model, with a discrete non linear spring elements, which can be viewed as point decohesion elements, are used to model the effect of stitches. Indeed, spring elements behaviour law is defined in section (Stitch model) as an elasto-plastic no compression law. The FE model is using 1440 decohesion elements along the length of the specimen. The arms are meshed by a regular quadrilateral plane strain element where, the selected element size is 0.1x0.1mm. The boundary conditions are applied by suppressing the degrees of freedom at the bottom end of the left beam. The imposed displacement is applied to the top right ends arms. The final material properties used in this correlation process are listed in tables 2 and 3 for elastic lamina properties and cohesive zone parameters.

Table 2. DCB specimen material constants

$E_1=E_2$ (GPa)	E_3 (GPa)	ν_{12}	$\nu_{13}=\nu_{23}$	G_{12} (GPa)	$G_{13}=G_{23}$ (GPa)
21.6	9.00	0.18	0.22	4.66	2.33

Table 3. Cohesive zone model parameters

G_{Ic} (N/mm)	k_n (N/mm^3)	t_2^0 (MPa)
0.9	10^6	50

As discussed above the delamination experiments were designed to study and record pure mode crack growth. G_{Ic} was taken as input to cohesive zone model. The maximum interlaminar traction t_2^0 was taken $t_2^0 = 50MPa$, it has been estimated from $(F-U)$ experimental curve. This value cannot be validated fully by experimental test where it is difficult to define exactly the onset traction of a delamination.

The simulations are performed by varying the stitches parameters denoted yield coordinates (ε_y, σ_y) and failure coordinates (ε_r, σ_r), characterizing the complete failure of the thread. The yield coordinates (ε_y, σ_y) have a little effect on force-displacement for the DCB specimen in this reason, the yield coordinates are maintained constant and their values can be determined by the microscopic properties of fibre and the interface fibre/matrix. For this case $(\varepsilon_y, \sigma_y) = (0.016, 6.28MPa)$.

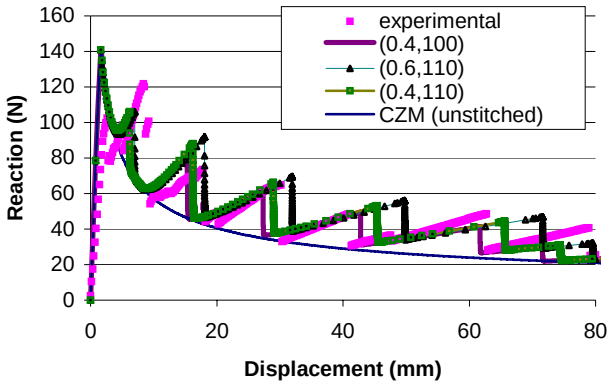

Fig. 9. Comparison of reaction vs. displacement simulation results with an experimental curve for mode I.

Fig. 9. compares the reaction versus cross-head displacement results with the corresponding observations. We denoted as the value of (ε_y, σ_y) is increased, the maximum load reached that corresponds to crack arrest at the first stitch increases. In addition, in the reinforced region an increases in delamination resistance is observed if we compare (force-displacement) of DCB specimen modelled with a cohesive zone model (unstitched) and for DCB specimen reinforced through the thickness. In the Fig. 9 and the phase of initiation (beginning of the softening of the curve) one notices a great difference between the numerical results and those obtained in experiments. Indeed, the phase of crack initiation can depend on several parameters for example thickness of the Teflon film and DCB sample geometry. However, in the phase of propagation, one notices a good correlation between simulation and the experimental one.

6. Conclusion

In this paper we studied the problem of the effect of mode I fracture toughness in the laminates composites. In the first part, we present the multi-scale stitch model concluding that a no compression elasto-plastic brittle law rather representative of the stitching effect. In the continuation, we defined a cohesive model with a bilinear softening law for the modelling of the initiation and the propagation of delamination in mixed mode. This model is used for the simulation of the interlaminar fracture toughness for the unstitched DCB specimen. In order to take account of the stitching effect in DCB samples, we

used a behaviour law defined previously as law of a spring element placed on the interface level.

In the experimental part, we established interlaminar fracture toughness tests in mode I for stitched and unstitched DCB specimens. From the test results we have to show that stitching increases the interlaminar fracture toughness but it doesn't affect the initiation of damage.

The comparison made between simulations and the results of the interlaminar resistance tests showed a good correlation in the phase of propagation but, a notable difference in the phase of initiation due probably to the geometrical conditions of the DCB test. Finally, it has been demonstrated through mode I fracture toughness simulations that the micro properties of stitch model (yield (ε_y, σ_y) and failure coordinates) can influence significantly the overall response at the structural level.

Acknowledgements

The authors would like to thank our French industrial partner "Direction de la Construction Navale (DCN)" for their contribution and helpful. The comments by Dr Patrick Parneix led to many useful improvements in the manuscript and is gratefully acknowledged.

References

[1] Jain L.K., Dransfield K. A. and Mai Y.-W. "On the effects of stitching in CFRPs-II. Mode II delamination toughness". *Composites Science and Technology*, Vol. 1, No. 58, pp 829-837, 1998.

[2] Tanzawa Y.; Watanabe N. and Ishikawa T. "FEM simulation of a modified DCB test for 3-D orthogonal interlocked fabric composites". *Composites Science and Technology*. Vol. 1, No. 61, pp 1097-1107, 2001.

[3] Velmurugan R. and Solaimurugan S. "Improvements in mode I interlaminar fracture toughness and in-plane mechanical properties of stitched glass/polyester composites". *Composites Science and Technology*. In Press, Corrected Proof, available online, 2006.

[4] Mourtiz A. P.; Baini C. and Herszberg I. "Mode I interlaminar fracture toughness properties of advanced textile fibreglass composites". *Composites Part A*. Vol. 1, No. 30, pp 859-870, 1999.

[5] Hamitouche L., Tarfaoui M. and Vautrin A. "Finite element interface debonding law subjected to viscous regularization for avoiding instability". *Mechanics of Material*. Submitted artcile, 2007.

[6] ABAQUS 2004 V6.5. User's Manual. Rising Sun Mills, USA: ABAQUS Inc.

[7] Geubelle P. H. and Baylor J. S. "Impact-induced delamination of composites: a 2d simulation". *Composites Part B*, No. 29B, pp 589-602, 1998.

[8] Mazars J. Application de la mécanique de l'endommagement au comportement non-linaire et la rupture du béton de structure. *PhD thesis*, Université de Paris6, 61, Av. PDT Wilson - 94230 Cachan - France, 1984.

[9] Turon A., Davila C. G., Camanho P. P., and Costa J. An engineering solution for using coarse meshes in the simulation of delamination with cohesive zone model. *Technical Memorandum*-2005-213547, NASA Langley Research Center, 2005.

[10] Reeder JR. An evaluation of mixed-Mode delamination failure criteria. *Technical Memorandum*-1992-104210, NASA Langley Research Center, 1992.

[11] ASTM D 5528-94a. Standard test method for Mode I interlaminar fracture toughness of unidirectional fibre-reinforced polymer matrix composites. *Annual book of ASTM standards*, Vol. 15.03, 1997.